

# Predictability of the upper ocean heat content in a Community Earth System Model ensemble prediction system

Ting Liu<sup>1, 2</sup>, Wenxiu Zhong<sup>1, 2, 3\*</sup>

<sup>1</sup> State Key Laboratory of Satellite Ocean Environment Dynamics, Second Institute of Oceanography, Ministry of Natural Resources, Hangzhou 310012, China

<sup>2</sup> Southern Marine Science and Engineering Guangdong Laboratory (Zhuhai), Zhuhai 519082, China

<sup>3</sup> School of Atmospheric Sciences, Sun Yat-Sen University, Zhuhai 519082, China

Received 19 July 2023; accepted 7 August 2023

© Chinese Society for Oceanography and Springer-Verlag GmbH Germany, part of Springer Nature 2024

## Abstract

Upper ocean heat content (OHC) has been widely recognized as a crucial precursor to high-impact climate variability, especially for that being indispensable to the long-term memory of the ocean. Assessing the predictability of OHC using state-of-the-art climate models is invaluable for improving and advancing climate forecasts. Recently developed retrospective forecast experiments, based on a Community Earth System Model ensemble prediction system, offer a great opportunity to comprehensively explore OHC predictability. Our results indicate that the skill of actual OHC predictions varies across different oceans and diminishes as the lead time of prediction extends. The spatial distribution of the actual prediction skill closely resembles the corresponding persistence skill, indicating that the persistence of OHC serves as the primary predictive signal for its predictability. The decline in actual prediction skill is more pronounced in the Indian and Atlantic oceans than in the Pacific Ocean, particularly within tropical regions. Additionally, notable seasonal variations in the actual prediction skills across different oceans align well with the phase-locking features of OHC variability. The potential predictability of OHC generally surpasses the actual prediction skill at all lead times, highlighting significant room for improvement in current OHC predictions, especially for the North Indian Ocean and the Atlantic Ocean. Achieving such improvements necessitates a collaborative effort to enhance the quality of ocean observations, develop effective data assimilation methods, and reduce model bias.

**Key words:** ocean heat content, prediction skill, retrospective forecast experiment

**Citation:** Liu Ting, Zhong Wenxiu. 2024. Predictability of the upper ocean heat content in a Community Earth System Model ensemble prediction system. *Acta Oceanologica Sinica*, 43(1): 1–10, doi: 10.1007/s13131-023-2239-x

## 1 Introduction

The predictability of upper ocean heat content (OHC) is a fascinating research area that provides valuable insights into climate dynamics, including oceanic processes and air-sea couplings (Wu et al., 2015). While atmospheric elements are highly sensitive to short-term perturbations with limited prediction skills of less than 1 month (Shukla, 1981), oceanic components retain long-term memories of air-sea interactions within the climate system due to thermal inertia (Li et al., 2017; Jian et al., 2022). As a representative of ocean subsurface processes, OHC possesses a longer memory and is more predictable than sea surface temperature (SST) (Branstator and Teng, 2010). Thus, OHC has been perceived as an effective predictor of climate variability, particularly for longer lead times in climate prediction (Jia and DelSole, 2011).

OHC variations in specific regions hold crucial information about climate variability and significant phenomena, such as the El Niño–Southern Oscillation (ENSO; Jin, 1997; Ren and Jin, 2013) and the Indian Ocean Dipole (IOD; Liu et al., 2022a). ENSO,

which comprises alternating warm El Niño and cool La Niña phases, substantially influences ecosystems, agriculture, and economies worldwide (McPhaden et al., 2006; Cai et al., 2015). Extensive research has been undertaken to improve the predictability of this critical climate phenomenon by investigating the relationship between OHC and ENSO (Clarke and van Gorder, 2003; McPhaden, 2003; Ham et al., 2019; Seleznev and Mukhin, 2023). Previous studies have shown that tropical Pacific warm water volume is closely correlated with ENSO variability, exhibiting a lead time of 6–9 months (Jin, 1997). Consequently, Pacific OHC has been identified as a potential precursor to ENSO events. Notably, OHC has demonstrated skillful forecasts for ENSO with lead times of up to 1 year (Tang et al., 2018; Zhang et al., 2022). Similarly, the Indian Ocean, with its distinctive characteristics, represents another region of interest concerning OHC and its impact on climate variability. IOD is a coupled ocean–atmosphere phenomenon characterized by SST anomalies between the western and eastern parts of the Indian Ocean (Saji et al., 1999). It has been suggested that Indian OHC can potentially influence the de-

Foundation item: The National Key R&D Program of China under contract No. 2020YFA0608803; the Scientific Research Fund of the Second Institute of Oceanography, Ministry of Natural Resources under contract No. QNYC2101; the National Natural Science Foundation of China under contract No. 42105052; the Fund of Southern Marine Science and Engineering Guangdong Laboratory (Zhuhai) under contract No. SML2021SP310; the Innovation Group Project of Southern Marine Science and Engineering Guangdong Laboratory (Zhuhai) under contract No. 311021001.

\*Corresponding author, E-mail: zhongwx9@mail.sysu.edu.cn

velopment and intensity of the IOD (Liu et al., 2022a). Therefore, it is crucial to understand the predictability of OHC for predicting the occurrence of high-impact climate events.

To improve the predictability of heat content, a comprehensive approach that integrates observational data and advanced numerical models is required. Improving the quality and resolution of ocean observations is essential for capturing heat content variations accurately. Developing and refining numerical models that simulate the intricate interactions between the atmosphere and ocean are also crucial for enhancing predictions. Recent advancements in data assimilation techniques have been promising in improving the predictability of oceanic variables. Furthermore, assimilating ocean observations into numerical models can help reduce uncertainties and enhance the accuracy of OHC predictions. Evaluating the OHC predictability in model simulations is crucial for further exploring climate variability.

The practical and intrinsic predictabilities are essential for evaluating predictability (Lorenz, 1965). The former represents the actual prediction skill and quantifies the accuracy of current predictions through the numerical model against observations. The latter is also known as potential predictability, indicating the upper limit of the prediction skill when the optimal procedure is used. Ensemble retrospective/hindcast forecasts based on state-of-the-art coupled models are powerful tools for understanding predictability. Recently, a long-term retrospective prediction based on the Community Earth System Model (CESM) was performed (Liu et al., 2022b). It provides a unique opportunity to explore a wide range of predictability problems regarding the climate system. In this study, we employed this retrospective ensemble forecast covering the 1880–2017 period to comprehensively investigate the OHC predictability. The remainder of this paper is organized as follows. Section 2 presents a detailed description of the retrospective forecasts and measurement metrics used. Sections 3 and 4 describe practical and intrinsic predictability traits, respectively. Finally, we provide a summary and in-depth discussion of the findings in Section 5.

## 2 Data and method

In this study, the long-term hindcast retrospective forecasts from a recently developed ensemble prediction system based on the CESM (Liu et al., 2022b) are utilized to investigate OHC predictability in climate model simulations. The retrospective forecasts were initialized each January 1st, April 1st, July 1st, and October 1st from 1880 to 2017 by nudging the ocean temperature at each depth above 500 m and wind at heights below 500 hPa (Song et al., 2022). The observational ocean temperature and winds nudging into the model are merged by different datasets. For the oceanic data, we used the monthly simple ocean data assimilation version 2.2.4 (SODA 2.2.4; Carton and Giese, 2008) before 1983 and the global ocean data assimilation system (GODAS; Behringer and Xue, 2004) datasets after 1983. Moreover, the 6-hourly ERA-20C reanalysis (Stocker et al., 2014) before 1983 and the ERA-interim reanalysis (Berrisford et al., 2011) after 1983 were used in nudging the observed atmospheric data into the model simulations. For any given start month, 20-member ensemble predictions were generated by the climatically relevant singular vector (Kleeman et al., 2003). All ensemble retrospective forecasts were run for 12 months. These ensemble integrations were produced to manifest the uncertainty in forecasts from the perturbed initial conditions of subsurface ocean temperature fields. We used the merged ocean temperatures from the SODA and GODAS datasets to evaluate the prediction skill of global OHC in the CESM hindcast retrospective forecasts.

The anomalies were calculated by subtracting the corres-

ponding climatology of the running 20-year window at each lead month to eliminate the impacts of decadal climate background and seasonal cycle in the prediction and observations. We used the standard deviation of the regional averaged OHC anomalies to represent the phase-locking features of OHC variability.

To estimate the actual prediction skills of the OHC, we employed the anomaly correlation coefficients (ACCs), which can be defined as

$$\text{ACC}(t) = \frac{\sum_{i=1}^N [H_i^o(t) - \overline{H^o}(t)] [H_i^f(t) - \overline{H^f}(t)]}{\sqrt{\sum_{i=1}^N [H_i^o(t) - \overline{H^o}(t)]^2} \sqrt{\sum_{i=1}^N [H_i^f(t) - \overline{H^f}(t)]^2}}, \quad (1)$$

where  $H$  denotes the OHC variable;  $f$  and  $o$  represent the ensemble mean prediction and observations, respectively;  $i$  and  $t$  are the initial and lead time of the forecast, respectively;  $N$  denotes the total number of initial conditions (138 years  $\times$  4 months). The overbar denotes the averaged value of multiple initial conditions.

We used information-based metrics to quantify the potential prediction skills of OHC, i.e., relative entropy (RE). RE measures the extra information from the predicted distribution over the climatological distribution (Kleeman, 2002), and it is given by

$$\text{RE}(i) = \frac{1}{2} \left[ \ln \left( \frac{\sigma_H^2}{\sigma_{H|i}^2} \right) + \frac{\sigma_{H|i}^2}{\sigma_H^2} - 1 + \frac{(\mu_{H|i} - \mu_H)^2}{\sigma_H^2} \right], \quad (2)$$

where  $\sigma_{H|i}^2$  and  $\sigma_H^2$  indicate the ensemble variance and climatological variance respectively.  $\mu_{H|i}$  and  $\mu_H$  denote the ensemble mean and climatological mean, respectively. The transformation of RE was used to measure the potential correlation (DelSole, 2004; Tang et al., 2013), which is given by

$$\text{ACC}_p = \sqrt{1 - e^{-2\text{RE}}}, \quad (3)$$

which implies  $\text{ACC}_p$  with a maximum value of 1 when the mean RE for all individual predictions approaches infinity and a minimum value of 0 when the mean RE vanishes.

## 3 Results

### 3.1 Actual predictability

Figure 1 demonstrates the spatial distribution of the ACC of OHC for all initial condition months with different lead months. The ACC skills vary with regions and decrease with increasing lead time. The skills are larger than 0.5 for a 1-month lead in most regions all over the globe (Fig. 1a). For a 2-month lead, the skills degenerate sharply in the tropical Indian and Atlantic oceans with ACC values smaller than 0.5. As with increasing lead time, the skill with a value larger than 0.5 appears only in the Pacific Ocean, which can even exceed 8 months in the tropical western Pacific Ocean and the southern Pacific Ocean (Fig. 1h). However, the skill with a value larger than 0.5, vanishes in the Indian and Atlantic oceans when the lead month exceeds five. This indicates that the Pacific OHC is more predictable than the Indian and Atlantic OHCs.

Figure 2 shows the spatial distribution pattern of the persistence skill of OHC, which is similar to that for ACC of CESM pre-

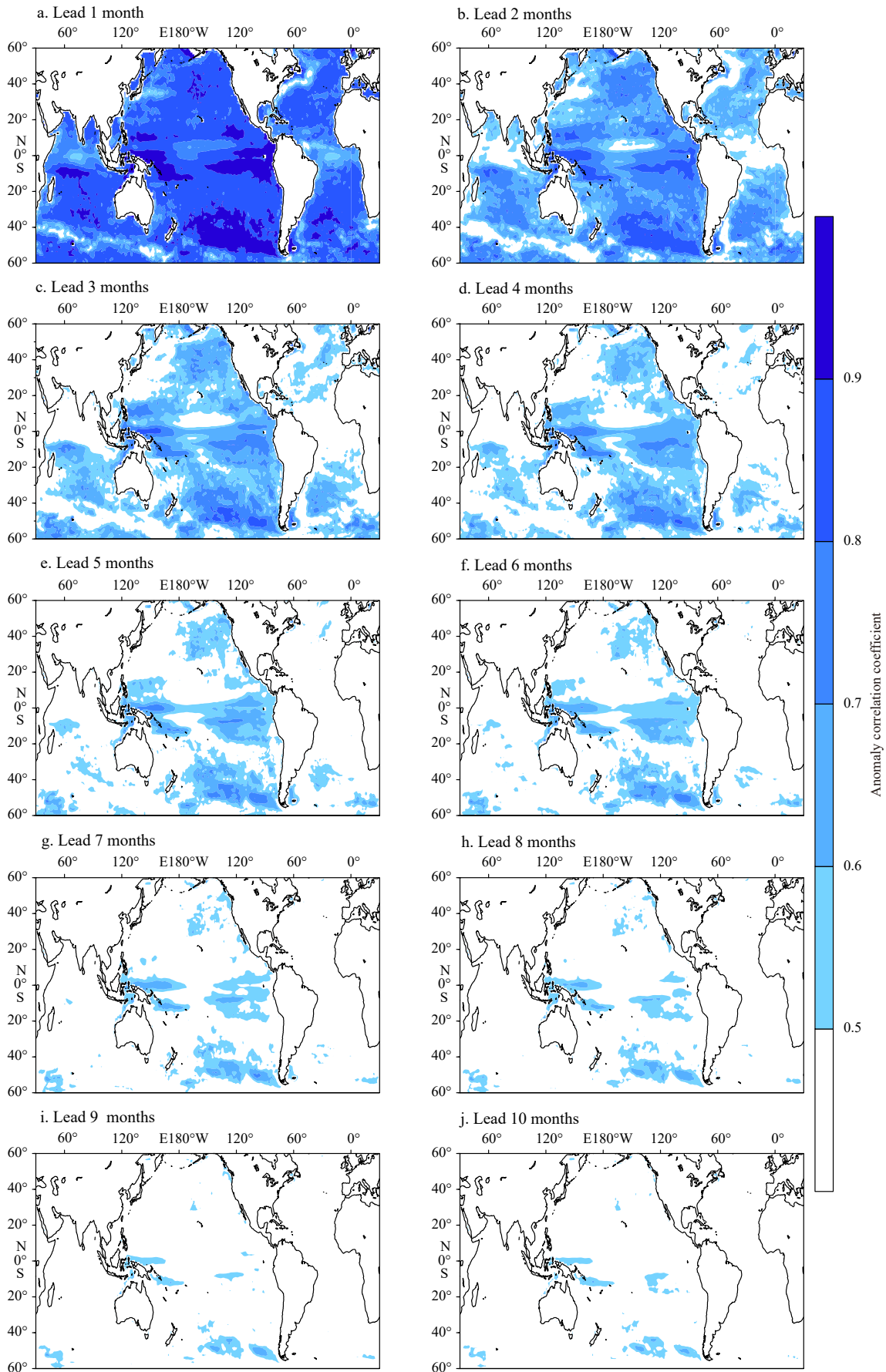


Fig. 1. Anomaly correlation coefficients of OHC with lead month.

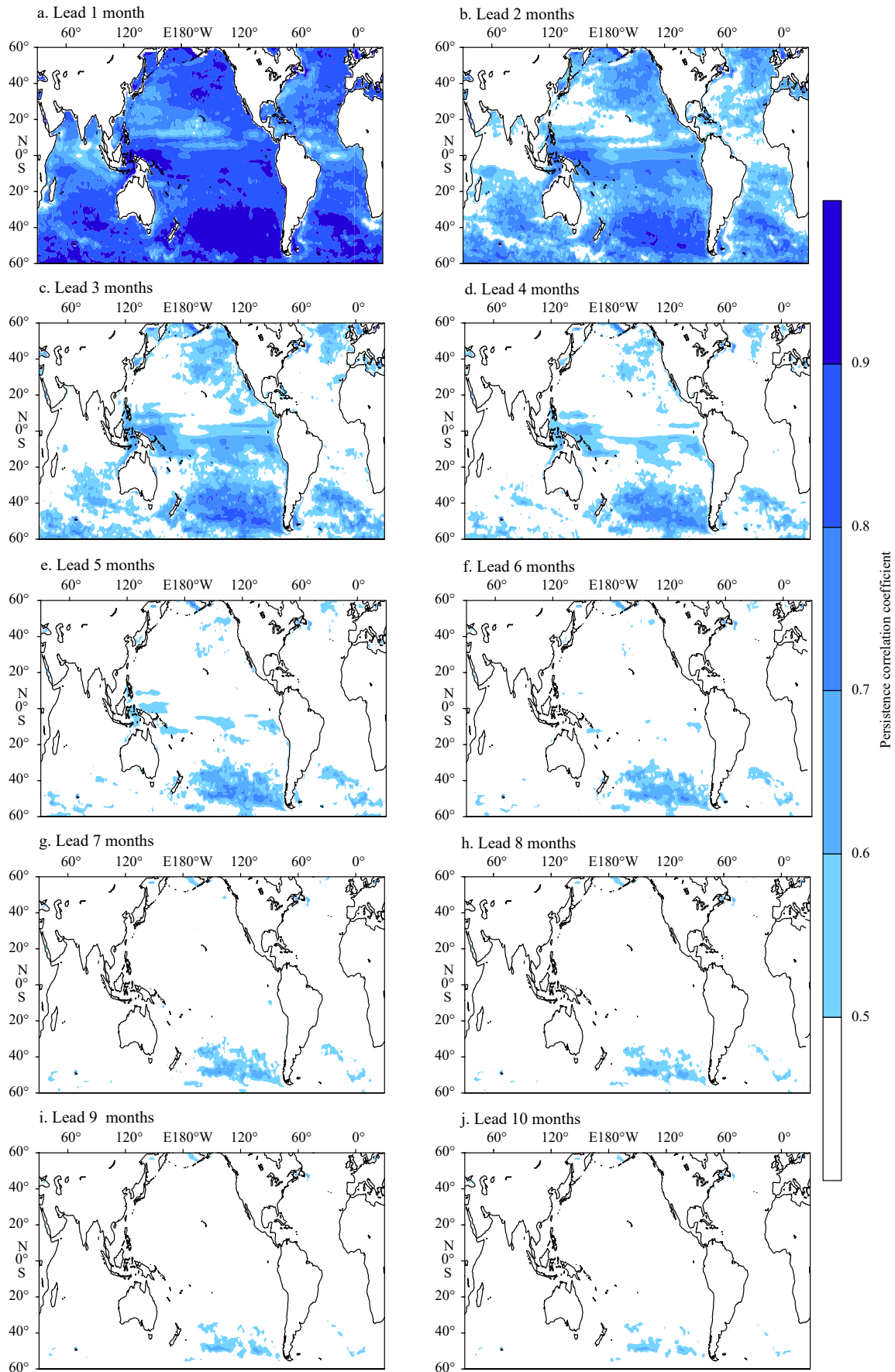
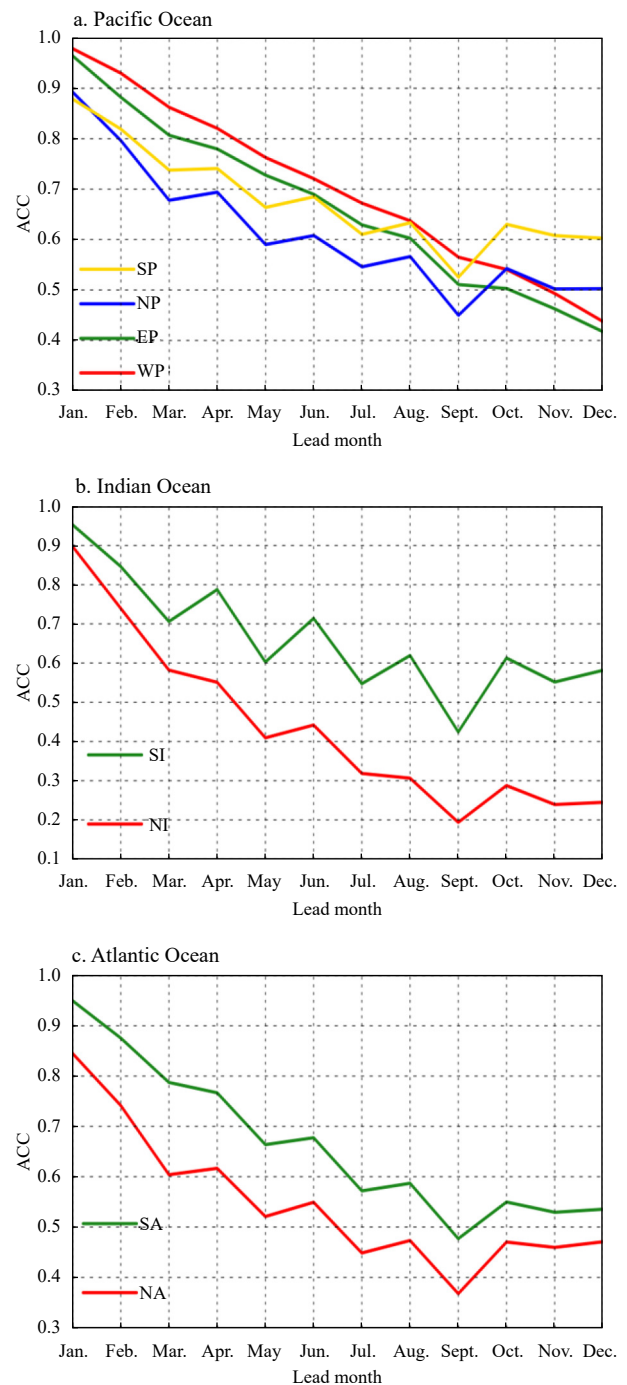


Fig. 2. Persistence coefficients of OHC with lead month.

diction. These overall similarities indicate that the persistence of OHC significantly contributes to its predictability. The ACC skills are inferior to the persistence skills in the middle and high latitudes for a 1-month lead, especially in the Southern Ocean. We speculate that two factors may account for this feature. One is the initial shock, documented for its influence on prediction skills (Chen, 2010). Another may be due to biases in the climate model or oceanic assimilation, which requires further examination. However, the model prediction exhibits clear superiority over persistence in most regions for lead times longer than 2 months. In addition, the lead time of the OHC in the tropical southwestern Indian Ocean is up to 5 months, much longer than that with persistence (Figs 1 and 2). These features indicate that the ensemble prediction system performs reasonably well in predicting OHC variability.

The predictability of OHC varies with regions in each ocean basin. As mentioned above, the Pacific OHC is more predictable than the Indian and Atlantic OHC. Next, we independently investigate the ACC skill of the OHC in different ocean areas (Fig. 3). In the Pacific Ocean, the ACC skill of OHC is higher in the tropics than in the middle and high latitude regions, with the highest and relatively high skills in the tropical western and eastern Pacific, respectively (Fig. 3a). This represents the canonical ENSO variance, indicating that the ENSO contributes significantly to the high predictability of OHC in the tropical Pacific Ocean than that in other ocean regions. In addition, its persistence is weaker in the northern Pacific Ocean than in the southern part. This leads to lower ACC skills in the northern Pacific Ocean than in the southern part. Meanwhile, in the Atlantic Ocean, the ACC skill is higher in the south than in the north. This is also related to the difference in persistence between these two regions, with higher persistence in the southern Atlantic Ocean than in the southern part (Fig. 3b). Asymmetric ACC with respect to the equator can be observed in the Indian Ocean, featuring significantly lower prediction skill in the northern sector than that in the southern counterpart (Figs 1, 3c). This is principally because of the relatively lower persistence in the northern Indian Ocean, which is potentially affected by monsoon systems (Shankar et al., 2002).

Similar to many other atmospheric and oceanic variables (Li and Ding, 2008, 2013), the ACC skill of the OHC also exhibits prominent seasonal variations. Figure 4 shows the ACC skill of the averaged OHC as a function of the target month and lead time in different ocean areas. Overall, the seasonal variation of the ACC skill varies with region. In the western and eastern Pacific, the highest ACCs occur in the target month of winter and spring, regardless of lead months (Figs 4a and b). This is well consistent with the phase locking of the OHC variability in the corresponding regions (Figs 5a and b). Meanwhile, in the northern and southern Pacific Ocean, the highest ACCs occur in the target month of July–October and January–April regardless of lead months, respectively (Figs 4c and d), which also generally corresponds to the phase locking of the OHC variability in these regions (Figs 5c and d). In the northern and southern Indian Ocean, the highest ACCs are also consistent with the highest variance of the OHC that appears in the target month of winter and spring (Figs 4e and f, Figs 5e and f). The phase-locking feature resembles that in the Pacific Ocean, indicating a significant correlation between the Pacific and the Indian oceans. In the northern and southern Atlantic oceans, the seasonal variation of the ACC is also consistent with the phase-locking feature of the OHC vari-



**Fig. 3.** Anomaly correlation coefficients (ACC) for the area-averaged OHC in the Pacific Ocean (a), Indian Ocean (b), and Atlantic Ocean (c). The “EP”, “WP”, “NP”, “SP”, “SI”, “NI”, “SA” and “NA” represent the eastern tropical Pacific ( $10^{\circ}\text{S}$ – $10^{\circ}\text{N}$ ,  $170^{\circ}\text{W}$ – $90^{\circ}\text{W}$ ), the western tropical Pacific ( $10^{\circ}\text{S}$ – $10^{\circ}\text{N}$ ,  $120^{\circ}\text{E}$ – $180^{\circ}$ ), the northeastern subtropical Pacific ( $20^{\circ}\text{N}$ – $60^{\circ}\text{N}$ ,  $180^{\circ}$ – $120^{\circ}\text{W}$ ), the southern Pacific ( $20^{\circ}\text{S}$ – $60^{\circ}\text{S}$ ,  $180^{\circ}$ – $90^{\circ}\text{W}$ ), the southern Indian Ocean ( $10^{\circ}\text{S}$ – $40^{\circ}\text{S}$ ,  $40^{\circ}\text{E}$ – $120^{\circ}\text{E}$ ), the northern Indian Ocean ( $10^{\circ}\text{N}$ – $25^{\circ}\text{N}$ ,  $50^{\circ}\text{E}$ – $110^{\circ}\text{E}$ ), the southern Atlantic Ocean ( $10^{\circ}\text{S}$ – $60^{\circ}\text{S}$ ,  $80^{\circ}\text{W}$ – $0^{\circ}$ ), and the northern Atlantic Ocean ( $10^{\circ}\text{N}$ – $60^{\circ}\text{N}$ ,  $60^{\circ}\text{W}$ – $0^{\circ}$ ), respectively.

ability in the corresponding regions (Figs 4g and h, Figs 5g and h). The synchronization between the ACC’s seasonal variation

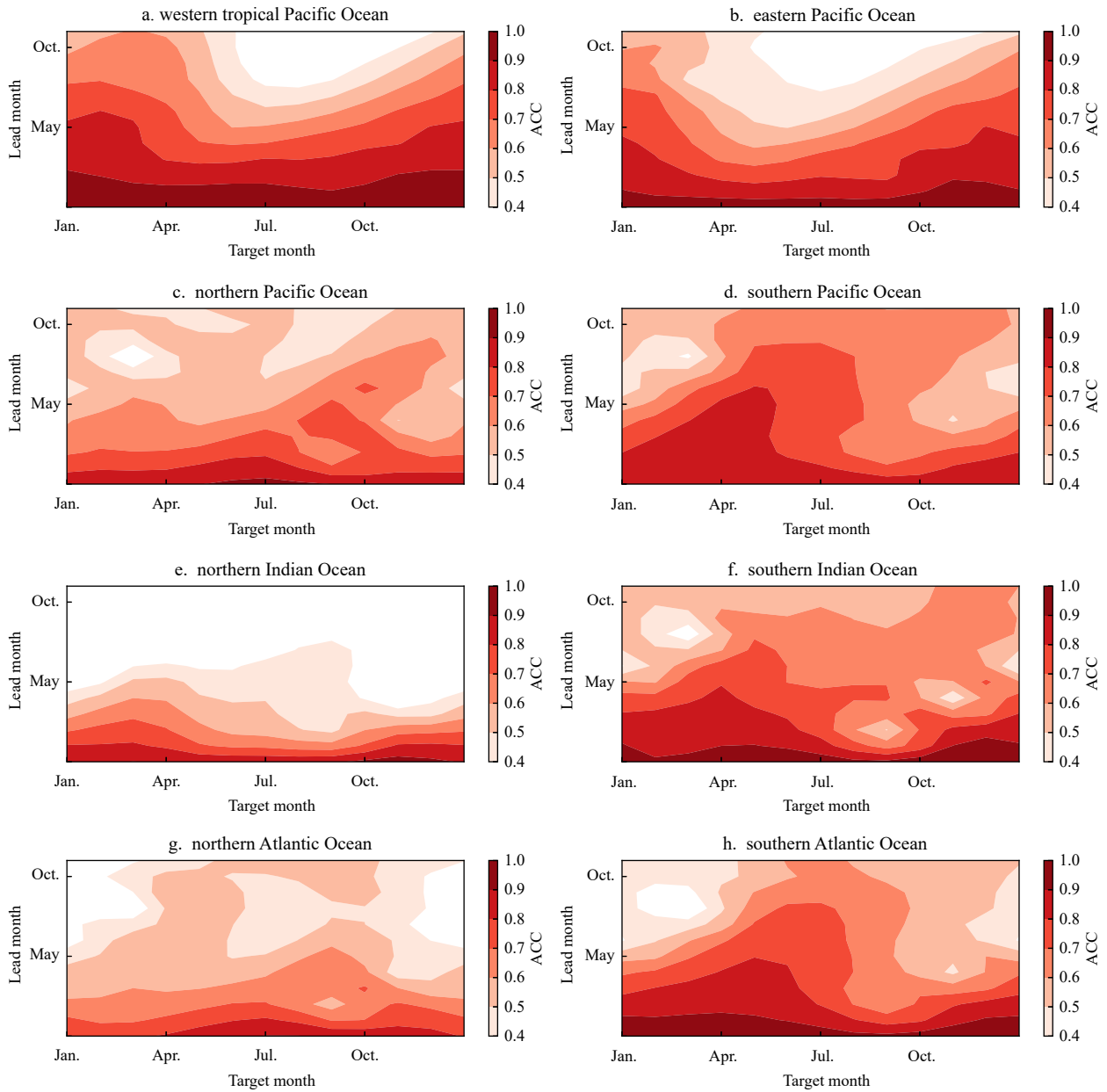


**Fig. 4.** Anomaly correlation coefficients (ACC) of the area-averaged OHC with the lead and target months in different oceans. a. The western tropical Pacific ( $10^{\circ}\text{S}$ – $10^{\circ}\text{N}$ ,  $120^{\circ}\text{E}$ – $180^{\circ}$ ); b. the eastern Pacific ( $10^{\circ}\text{S}$ – $10^{\circ}\text{N}$ ,  $170^{\circ}\text{W}$ – $90^{\circ}\text{W}$ ); c. the northern Pacific ( $20^{\circ}\text{N}$ – $60^{\circ}\text{N}$ ,  $180^{\circ}$ – $120^{\circ}\text{W}$ ); d. the southern Pacific ( $20^{\circ}\text{S}$ – $60^{\circ}\text{S}$ ,  $180^{\circ}$ – $90^{\circ}\text{W}$ ); e. the northern Indian Ocean ( $10^{\circ}\text{N}$ – $25^{\circ}\text{N}$ ,  $50^{\circ}\text{E}$ – $110^{\circ}\text{E}$ ); f. the southern Indian Ocean ( $10^{\circ}\text{S}$ – $40^{\circ}\text{S}$ ,  $40^{\circ}\text{E}$ – $120^{\circ}\text{E}$ ); g. the northern Atlantic Ocean ( $10^{\circ}\text{N}$ – $60^{\circ}\text{N}$ ,  $60^{\circ}\text{W}$ – $0^{\circ}$ ); h. the southern Atlantic Ocean ( $10^{\circ}\text{S}$ – $60^{\circ}\text{S}$ ,  $80^{\circ}\text{W}$ – $0^{\circ}$ ).

and the OHC variability's phase-locking indicate the OHC signal's dominant contribution to the prediction skill.

### 3.2 Potential predictability

Now that we have assessed the actual ability of the current model to predict OHC variability, one may wonder if our OHC prediction approach can be regarded as an approximation to the intrinsic predictability limit, which can be measured using the potential predictability metrics. Although the actual prediction skill measures the performance of the current climate model in predicting climate (or projecting future climate) variability against corresponding observations, potential predictability quantifies the upper limit of the actual skill assuming the model

is perfect, and does not use observations when quantifying it. Figure 6 illustrates the spatial distribution of the potential correlation of OHC with different lead months. Similar to the ACC skill, the potential correlation of OHC also varies across regions and decreases with increasing lead time. However, the decrease of the potential correlation is significantly slower than that of the ACC in most regions (Figs 1, 6). As potential predictability refers to the ideal skill we could achieve, the gap between the potential predictability and actual prediction skill is often considered as substantial room for further improvement in current predictions. Figure 7 shows the difference between the potential correlation and ACC of OHC with different lead months. We notice that the potential skill is consistently higher than the actual skill for all

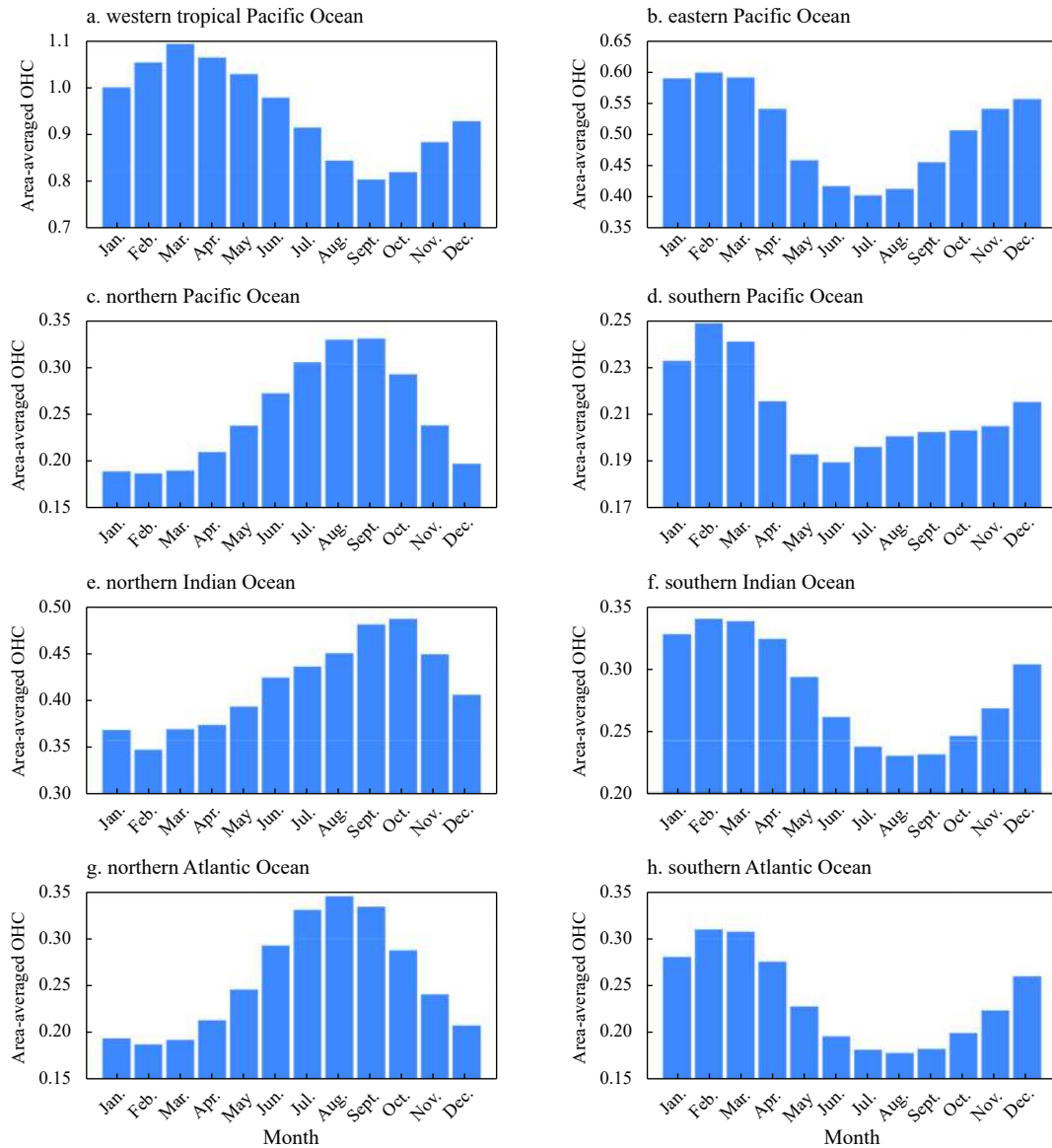


**Fig. 5.** Phase-locking features of the area-averaged OHC in different oceans. a. The western tropical Pacific ( $10^{\circ}\text{S}$ – $10^{\circ}\text{N}$ ,  $120^{\circ}\text{E}$ – $180^{\circ}$ ); b. the eastern Pacific ( $10^{\circ}\text{S}$ – $10^{\circ}\text{N}$ ,  $170^{\circ}\text{W}$ – $90^{\circ}\text{W}$ ); c. the northern Pacific ( $20^{\circ}\text{N}$ – $60^{\circ}\text{N}$ ,  $180^{\circ}$ – $120^{\circ}\text{W}$ ); d. the southern Pacific ( $20^{\circ}\text{S}$ – $60^{\circ}\text{S}$ ,  $180^{\circ}$ – $90^{\circ}\text{W}$ ); e. the northern Indian Ocean ( $10^{\circ}\text{N}$ – $25^{\circ}\text{N}$ ,  $50^{\circ}\text{E}$ – $110^{\circ}\text{E}$ ); f. the southern Indian Ocean ( $10^{\circ}\text{S}$ – $40^{\circ}\text{S}$ ,  $40^{\circ}\text{E}$ – $120^{\circ}\text{E}$ ); g. the northern Atlantic Ocean ( $10^{\circ}\text{N}$ – $60^{\circ}\text{N}$ ,  $60^{\circ}\text{W}$ – $0^{\circ}$ ); h. the southern Atlantic Ocean ( $10^{\circ}\text{S}$ – $60^{\circ}\text{S}$ ,  $80^{\circ}\text{W}$ – $0^{\circ}$ ).

lead times. Moreover, this gap increases as the lead time extends, indicating significant room for improvement in the prediction of OHC, especially for long lead times. The improvement for the Atlantic Ocean is also more urgent than the Pacific and Indian oceans, which is regarded as a crucial driver of multiple inter-basin interactions (Cai et al., 2019). Moreover, the Atlantic OHC has been proposed to be related to changes in the Atlantic Meridional Overturning Circulation and wind-driven circulation that transport ocean heat globally (Robson et al., 2012; Jackson et al., 2016; Piecuch et al., 2017; Bersch, 2002; Josey and Sinha, 2022).

#### 4 Conclusions and discussion

OHC has been consistently recognized as a crucial potential precursor to high-impact climate events worldwide, making it an effective predictor of long-term climate variability. Consequently, the predictability of OHC becomes a key objective in operational climate forecasts, with significant implications for mitigating cli-

mate disasters. Although the predictability of SST has made groundbreaking progress in recent decades, our understanding of OHC predictability remains relatively deficient. Fortunately, recently developed retrospective forecast experiments, based on a CESM ensemble prediction system, offer an excellent opportunity to comprehensively explore OHC predictability. Our results indicate that the actual prediction skill varies across different oceans and decreases with increasing lead time. Interestingly, the spatial distribution of the actual prediction skill closely resembles that of the corresponding prediction skill, suggesting that the persistence of OHC serves as the primary predictive signal for its predictability.

The actual prediction skill decreases sharply in the Indian and Atlantic oceans than in the Pacific Ocean, especially in the tropics. In the Pacific Ocean, the actual prediction skill is higher in the tropics than in the middle and high latitudes, with the highest and relatively high skills observed in the tropical western

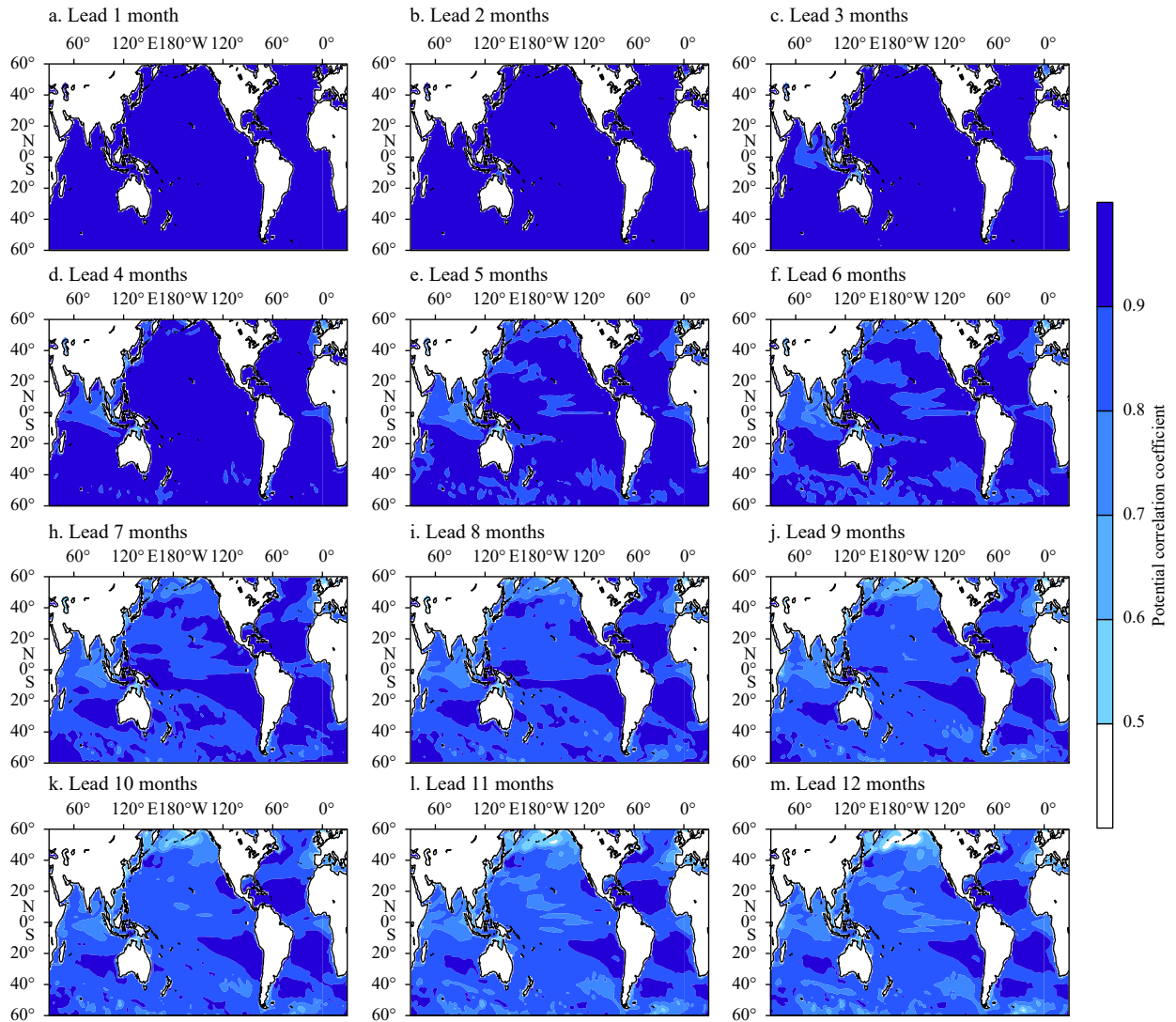


Fig. 6. Potential correlation of OHC with lead month.

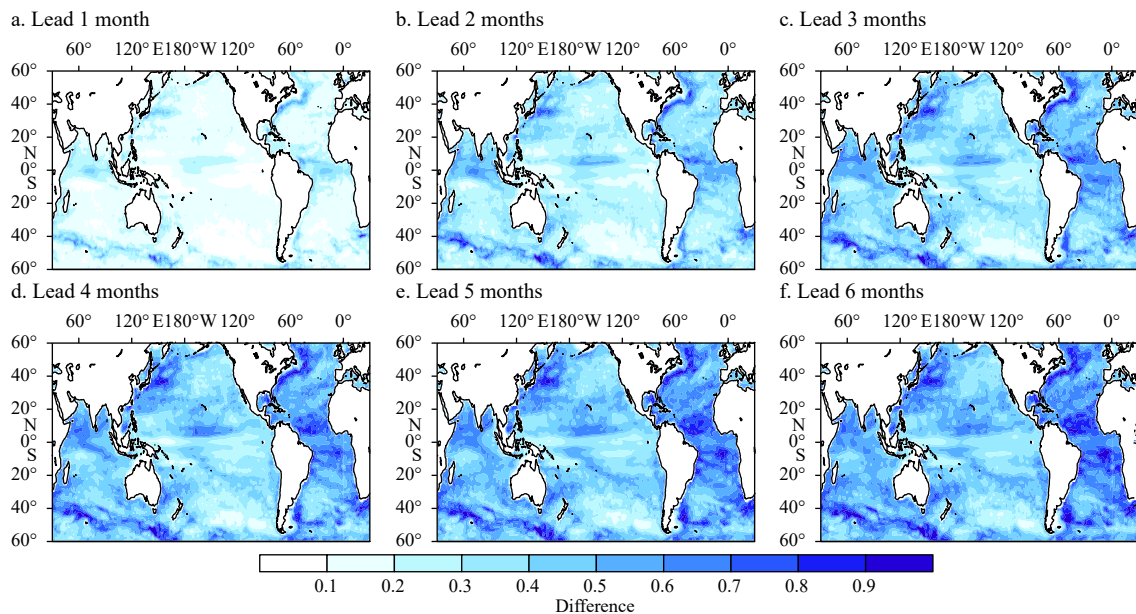


Fig. 7.

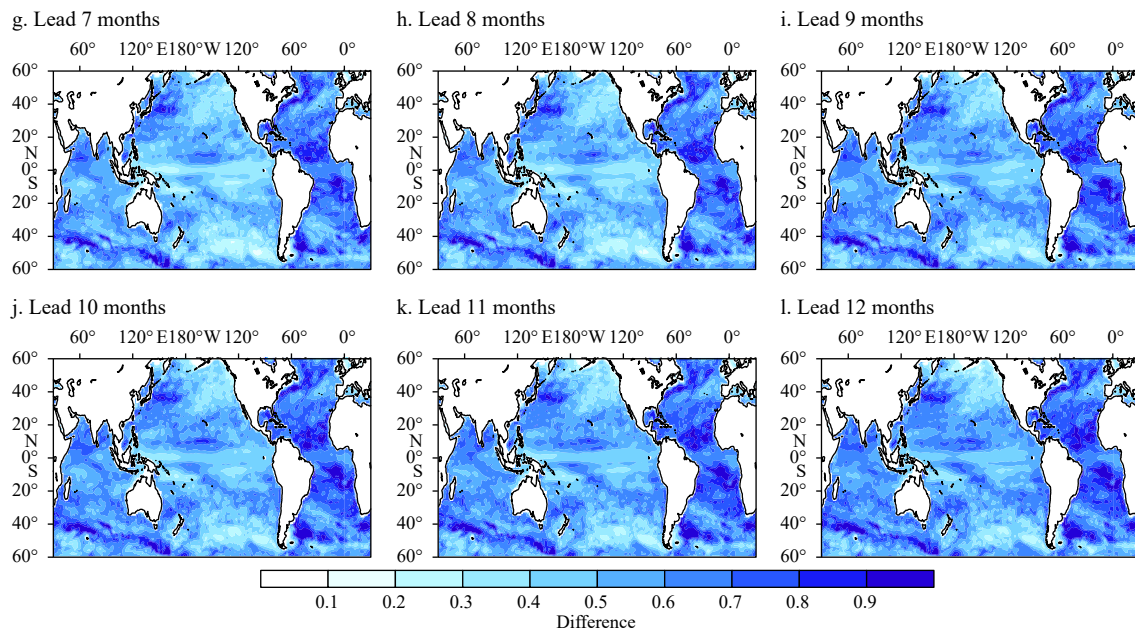


Fig. 7. Difference between the potential correlation and the anomaly correlation coefficients of OHC with lead month.

and eastern Pacific due to the influence of ENSO. In addition, the higher persistence of OHC in the southern Pacific Ocean contributes to higher actual prediction skills in this region than in the northern part. However, the situation in the Indian and Atlantic oceans differs significantly, with higher actual prediction skills in the middle and high latitudes than in the tropics. Similarly, the higher persistence of OHC in the southern Indian Ocean and Atlantic Ocean also contributes to higher actual prediction skills in these regions than in their northern part. Moreover, significant seasonal variations in the actual prediction skills are observed in different oceans, which agree well with the corresponding phase locking of the OHC variability. This further indicates that the OHC signal plays a dominant role in the prediction skill.

The potential predictability of OHC is generally higher than the actual prediction skill in all lead times, indicating significant room for improvement in the existing OHC predictions, especially for the Atlantic Ocean and long lead times. Achieving such improvement requires a collaborative effort to enhance the quality of ocean observations, develop effective data assimilation methods, and minimize model bias. Furthermore, understanding the interdecadal variation of predictability is crucial for comprehending the interdecadal variability of high-impact climate events. A related study addressing this aspect is currently underway.

## References

- Behringer D, Xue Yan. 2004. Evaluation of the global ocean data assimilation system at NCEP: The Pacific Ocean. In: Proceedings of the Eighth Symposium on Integrated Observing and Assimilation Systems for Atmosphere, Oceans, and Land Surface. Seattle, WA: American Meteorological Society
- Berrisford P, Dee D P, Poli P, et al. 2011. The ERA-Interim Archive: Version 2.0. ERA Report Series, 1: 23
- Bersch M. 2002. North Atlantic Oscillation-induced changes of the upper layer circulation in the northern North Atlantic Ocean. *Journal of Geophysical Research: Oceans*, 107(C10): 3156, doi: [10.1029/2001JC000901](https://doi.org/10.1029/2001JC000901)
- Branstator G, Teng Haiyan. 2010. Two limits of initial-value decadal predictability in a CGCM. *Journal of Climate*, 23(23): 6292–6311, doi: [10.1175/2010JCLI3678.1](https://doi.org/10.1175/2010JCLI3678.1)
- Cai Wenju, Santoso A, Wang Guojian, et al. 2015. ENSO and greenhouse warming. *Nature Climate Change*, 5(9): 849–859, doi: [10.1038/nclimate2743](https://doi.org/10.1038/nclimate2743)
- Cai Wenju, Wu Lixin, Lengaigne M, et al. 2019. Pantropical climate interactions. *Science*, 363(6430): eaav4236, doi: [10.1126/science.aav4236](https://doi.org/10.1126/science.aav4236)
- Carton J A, Giese B S. 2008. A reanalysis of ocean climate using simple ocean data assimilation (SODA). *Monthly Weather Review*, 136(8): 2999–3017, doi: [10.1175/2007MWR1978.1](https://doi.org/10.1175/2007MWR1978.1)
- Chen Dake. 2010. Coupled data assimilation for ENSO prediction. In: Gan Jianping, ed. *Advances in Geosciences: Volume 18: Ocean Science (OS)*. New Jersey: World Scientific Publishing Company, 45–62
- Clarke A J, Van Gorder S. 2003. Improving El Niño prediction using a space-time integration of Indo-Pacific winds and equatorial Pacific upper ocean heat content. *Geophysical Research Letters*, 30(7): 1399
- DelSole T. 2004. Predictability and information theory. Part I: Measures of predictability. *Journal of the Atmospheric Sciences*, 61(20): 2425–2440, doi: [10.1175/1520-0469\(2004\)061<2425:PAITPI>2.0.CO;2](https://doi.org/10.1175/1520-0469(2004)061<2425:PAITPI>2.0.CO;2)
- Ham Y G, Kim J H, Luo Jingjia. 2019. Deep learning for multi-year ENSO forecasts. *Nature*, 573(7775): 568–572, doi: [10.1038/s41586-019-1559-7](https://doi.org/10.1038/s41586-019-1559-7)
- Jackson L C, Peterson K A, Roberts C D, et al. 2016. Recent slowing of Atlantic overturning circulation as a recovery from earlier strengthening. *Nature Geoscience*, 9(7): 518–522, doi: [10.1038/ngeo2715](https://doi.org/10.1038/ngeo2715)
- Jia Liwei, DelSole T. 2011. Diagnosis of multiyear predictability on continental scales. *Journal of Climate*, 24(19): 5108–5124, doi: [10.1175/2011JCLI4098.1](https://doi.org/10.1175/2011JCLI4098.1)
- Jian Zhimin, Wang Yue, Dang Haowen, et al. 2022. Warm pool ocean heat content regulates ocean–continent moisture transport. *Nature*, 612(7938): 92–99, doi: [10.1038/s41586-022-05302-y](https://doi.org/10.1038/s41586-022-05302-y)
- Jin Feifei. 1997. An equatorial ocean recharge paradigm for ENSO. Part I: Conceptual model. *Journal of Atmospheric Sciences*, 54(7): 811–829, doi: [10.1175/1520-0469\(1997\)054<0811:AEORPF>2.0.CO;2](https://doi.org/10.1175/1520-0469(1997)054<0811:AEORPF>2.0.CO;2)
- Josey S A, Sinha B. 2022. Subpolar Atlantic Ocean mixed layer heat content variability is increasingly driven by an active ocean. *Communications Earth and Environment*, 3(1): 111, doi: [10.1038/s43247-022-00433-6](https://doi.org/10.1038/s43247-022-00433-6)
- Kleeman R. 2002. Measuring dynamical prediction utility using relative entropy. *Journal of the Atmospheric Sciences*, 59(13):

- 2057–2072, doi: [10.1175/1520-0469\(2002\)059<2057:MDPUUR>2.0.CO;2](https://doi.org/10.1175/1520-0469(2002)059<2057:MDPUUR>2.0.CO;2)
- Kleeman R, Tang Youmin, Moore A M. 2003. The calculation of climatically relevant singular vectors in the presence of weather noise as applied to the ENSO problem. *Journal of the Atmospheric Sciences*, 60(23): 2856–2868, doi: [10.1175/1520-0469\(2003\)060<2856:TCOCRS>2.0.CO;2](https://doi.org/10.1175/1520-0469(2003)060<2856:TCOCRS>2.0.CO;2)
- Li Jianping, Ding Ruiqiang. 2008. Temporal-spatial distributions of predictability limit of short-term climate. *Chinese Journal of Atmospheric Sciences (in Chinese)*, 32(4): 975–986
- Li Jianping, Ding Ruiqiang. 2013. Temporal-spatial distribution of the predictability limit of monthly sea surface temperature in the global oceans. *International Journal of Climatology*, 33(8): 1936–1947, doi: [10.1002/joc.3562](https://doi.org/10.1002/joc.3562)
- Li Shujun, Zhang Liping, Wu Lixin. 2017. Decadal potential predictability of upper ocean heat content over the twentieth century. *Climate Dynamics*, 49(9–10): 3293–3307, doi: [10.1007/s00382-016-3513-9](https://doi.org/10.1007/s00382-016-3513-9)
- Liu Minghong, McPhaden M J, Ren Hongli, et al. 2022a. Oceanic heat content as a predictor of the Indian Ocean Dipole. *Journal of Geophysical Research: Oceans*, 127(12): e2022JC018896, doi: [10.1029/2022JC018896](https://doi.org/10.1029/2022JC018896)
- Liu Ting, Song Xunshu, Tang Youmin, et al. 2022b. ENSO predictability over the past 137 years based on a CESM ensemble prediction system. *Journal of Climate*, 35(2): 763–777, doi: [10.1175/JCLI-D-21-0450.1](https://doi.org/10.1175/JCLI-D-21-0450.1)
- Lorenz E N. 1965. A study of the predictability of a 28-variable atmospheric model. *Tellus*, 17(3): 321–333, doi: [10.1111/j.2153-3490.1965.tb01424.x](https://doi.org/10.1111/j.2153-3490.1965.tb01424.x)
- McPhaden M J. 2003. Tropical Pacific Ocean heat content variations and ENSO persistence barriers. *Geophysical Research Letters*, 30(9): 1480, doi: [10.1029/2003GL016872](https://doi.org/10.1029/2003GL016872)
- McPhaden M J, Zebiak S E, Glantz M H. 2006. ENSO as an integrating concept in earth science. *Science*, 314(5806): 1740–1745, doi: [10.1126/science.1132588](https://doi.org/10.1126/science.1132588)
- Piecuch C G, Ponte R M, Little C M, et al. 2017. Mechanisms underlying recent decadal changes in subpolar North Atlantic Ocean heat content. *Journal of Geophysical Research: Oceans*, 122(9): 7181–7197, doi: [10.1002/2017JC012845](https://doi.org/10.1002/2017JC012845)
- Ren Hongli, Jin Feifei. 2013. Recharge oscillator mechanisms in two types of ENSO. *Journal of Climate*, 26(17): 6506–6523, doi: [10.1175/JCLI-D-12-00601.1](https://doi.org/10.1175/JCLI-D-12-00601.1)
- Robson J, Sutton R, Lohmann K, et al. 2012. Causes of the rapid warming of the North Atlantic Ocean in the mid-1990s. *Journal of Climate*, 25(12): 4116–4134, doi: [10.1175/JCLI-D-11-00443.1](https://doi.org/10.1175/JCLI-D-11-00443.1)
- Saji N H, Goswami B N, Vinayachandran P N, et al. 1999. A dipole mode in the tropical Indian Ocean. *Nature*, 401(6751): 360–363
- Seleznev A, Mukhin D. 2023. Improving statistical prediction and revealing nonlinearity of ENSO using observations of ocean heat content in the tropical Pacific. *Climate Dynamics*, 60(1–2): 1–15, doi: [10.1007/s00382-022-06298-x](https://doi.org/10.1007/s00382-022-06298-x)
- Shankar D, Vinayachandran P N, Unnikrishnan A S. 2002. The monsoon currents in the north Indian Ocean. *Progress in Oceanography*, 52(1): 63–120, doi: [10.1016/S0079-6611\(02\)00024-1](https://doi.org/10.1016/S0079-6611(02)00024-1)
- Shukla J. 1981. Dynamical predictability of monthly means. *Journal of the Atmospheric Sciences*, 38(12): 2547–2572, doi: [10.1175/1520-0469\(1981\)038<2547:DPOMM>2.0.CO;2](https://doi.org/10.1175/1520-0469(1981)038<2547:DPOMM>2.0.CO;2)
- Song Xunshu, Li Xiaojing, Zhang Shouwen, et al. 2022. A new nudging scheme for the current operational climate prediction system of the National Marine Environmental Forecasting Center of China. *Acta Oceanologica Sinica*, 41(2): 51–64, doi: [10.1007/s13131-021-1857-4](https://doi.org/10.1007/s13131-021-1857-4)
- Stickler A, Brönnimann S, Valente M A, et al. 2014. ERA-CLIM: Historical surface and upper-air data for future reanalyses. *Bulletin of the American Meteorological Society*, 95(9): 1419–1430, doi: [10.1175/BAMS-D-13-00147.1](https://doi.org/10.1175/BAMS-D-13-00147.1)
- Tang Youmin, Chen Dake, Yang Dejian, et al. 2013. Methods of estimating uncertainty of climate prediction and climate change projection. In: Singh B R, ed. *Climate Change-Realities, Impacts over Ice Cap, Sea Level and Risks*. Rijeka: IntechOpen
- Tang Youmin, Zhang Ronghua, Liu Ting, et al. 2018. Progress in ENSO prediction and predictability study. *National Science Review*, 5(6): 826–839, doi: [10.1093/nsr/nwy105](https://doi.org/10.1093/nsr/nwy105)
- Wu Xiaofen, Liu Zenghong, Liao Guanghong, et al. 2015. Variation of Indo-Pacific upper ocean heat content during 2001–2012 revealed by Argo. *Acta Oceanologica Sinica*, 34(5): 29–38, doi: [10.1007/s13131-015-0664-1](https://doi.org/10.1007/s13131-015-0664-1)
- Zhang Ronghua, Gao Chuan, Feng Licheng. 2022. Recent ENSO evolution and its real-time prediction challenges. *National Science Review*, 9(4): nwac052, doi: [10.1093/nsr/nwac052](https://doi.org/10.1093/nsr/nwac052)